Electrochemistry
The Electrochemical Society of Japan
Received: August 29, 2022
Accepted: October 5, 2022
Published online: October 7, 2022
Issued: November 29, 2022
https://doi.org/10.5796/electrochemistry.22-00100
https://doi.org/10.50892/data.electrochemistry.21286026
Article
Electrochemistry, **90(11)**, 117005 (2022)

3,6-Diphenyltetrazine as Cathode Active Material for Sodium Ion Batteries†

Jun WATANABE,[a] Masaki FURUSAWA,[b,c] Kosuke NAKAMOTO,[b,c,§] Yuchao SUN,[a,d] Masatoshi TASHIMA,[a] Keiko YAMAOKA,[b] Seiko FUJIWARA,[b] Han Seul KIM,[a,e] Shigeto OKADA,[b,c,*,§§] and Ken ALBRECHT[b,c,f,*,§]

[a] *Interdisciplinary Graduate School of Engineering Sciences, Kyushu University, 6-1 Kasuga-Koen, Kasuga, Fukuoka 816-8580, Japan*
[b] *Institute for Materials Chemistry and Engineering, Kyushu University, 6-1 Kasuga-Koen, Kasuga, Fukuoka 816-8580, Japan*
[c] *Elements Strategy Initiative for Catalysts & Batteries (ESICB), Kyoto University, 1-30 Goryoohara, Nishikyo-ku, Kyoto 615-8245, Japan*
[d] *School of Materials Science and Engineering, Shanghai Jiao Tong University, 800 Dongchuan RD., Minhang District, Shanghai 200240, P. R. China*
[e] *Graduate School of Nanofusion Technology, Pusan National University, Busandaehak-ro 63beon-gil, Jangjeon2(i)-dong, Geumjeong-gu, Busan 46241, Republic of Korea*
[f] *JST-PRESTO, 4-1-8 Honcho, Kawaguchi, Saitama 332-0012, Japan*

* *Corresponding authors: s-okada@cm.kyushu-u.ac.jp (S. O.), albrecht@cm.kyushu-u.ac.jp (K. A.)*

ABSTRACT

3,6-diphenyltetrazine (DPT) is an electron-deficient π-conjugated molecule with a perfectly planar structure and high crystallinity. In this study, discharge-charge tests of crystalline DPT as a cathode material for sodium ion batteries were conducted. DPT showed an initial reversible capacity of 102 mAh/g (theoretical capacity 114 mAh/g), corresponding to one electron reaction. The plateau of the discharge-charge profiles was observed at 1.9–2.1 V vs. Na/Na$^+$. According to the ex-situ XRD, FT-IR, and XPS measurements to investigate the discharge-charge mechanism, the redox center was identified as the conjugated tetrazine ring. DPT was in a crystalline form in both the charged and discharged state and indicated the potential as a reversible Na ion host.

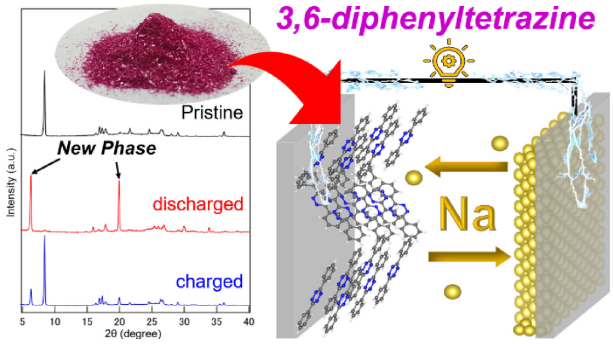

Keywords : Sodium Ion Battery, Organic Battery, Cathode Material, *s*-Tetrazine

1. Introduction

Secondary batteries such as lithium ion batteries (LIBs) have been widely used in several mobile electronic devices; however, alternative material (device) is eagerly anticipated due to the small reserve, high price, high environmental impact, and safety issues. Recently, the demand for LIBs is shifting to large storage batteries for electric vehicles and backup batteries for renewable energy that has large output fluctuations. The LIBs suffer from the high cost of lithium and the rare metals such as cobalt used as cathode material and the high environmental impact. One of the viable alternative materials that are attracting attention is sodium. The standard electrode potential of sodium is only 0.3 V higher than that of lithium, and sodium is abundant in seawater and salt deposits. It is superior in terms of economic efficiency and environmental impact and is highly expected as a post-LIB for large storage batteries.

Sodium ion batteries (SIBs) are one of the most promising alternatives to LIBs, but sodium ion is three times as bulky as lithium ion in terms of atomic weight and about twice as bulky in terms of ionic volume. In order to use sodium as a charge carrier in a battery, an electrode material with a crystalline structure with a sufficient diffusion path is required. Conventional positive electrode active materials for LIBs such as dense transition metal oxides are unsuitable for sodium ion storage. Organic compounds (redox groups) have been attracting attention as cathode material in SIB,[1,2] Because they have a low specific gravity that ensures sufficient diffusion of sodium ions in the electrode, high specific (weight) capacity, structural variation, and environmental sustainability. In the conventional organic electrode materials, C=O[3–10] is often used as the redox active group. However, exploring new redox active groups has become a trend for further development of organic electrode materials. Recently, the structural diversity of organic SIB cathode with double bond redox groups has been expanded to N=N,[11] C=N,[12,13] S=C,[14] and S=O.[15] These studies contribute to the elucidation of structure-property relationships and the development of design strategies for future high-performance organic SIBs.

s-Tetrazine[16] is an electron-deficient six-membered conjugated heterocycle with N=N and C=N bond and can be reversibly reduced by one electron to form a stable radical anion. Recently, *s*-Tetrazine was reported as active material as cathode for LIB.[17,18]

†A part of this paper has been presented in the 88th ECSJ Meeting in 2021 (Presentation #1L23).
§ECSJ Active Member
§§ECSJ Fellow

K. Nakamoto orcid.org/0000-0003-4398-6597
S. Okada orcid.org/0000-0002-8944-1990
K. Albrecht orcid.org/0000-0003-2159-2204

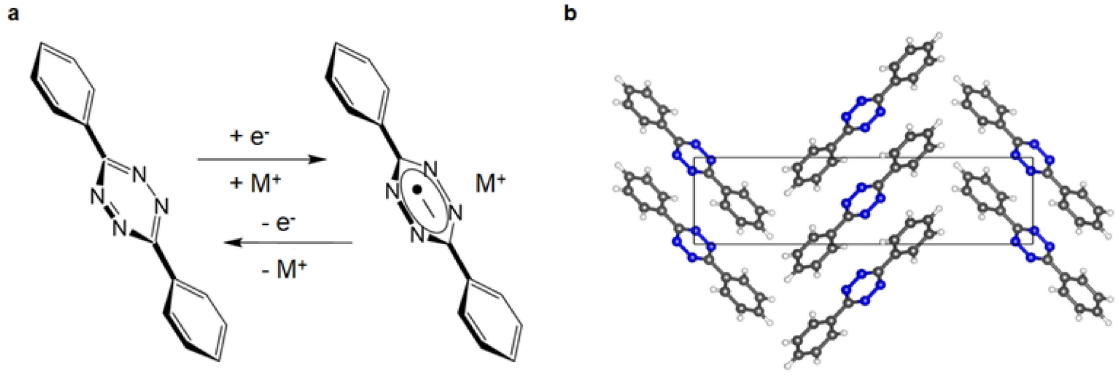

Figure 1. **a** Redox reaction of DPT. **b** Crystal structure of DPT.[21] Visualized with VESTA3[22] using single crystal X-ray data reported by R. Ranjbar-Karimi et al. (CCDC 1580478). The blue, gray, and white atoms represent nitrogen, carbon, and hydrogen. The Square black line indicates a single unit cell.

Among tetrazine derivatives, 3,6-dipehnyltetrazine (DPT) was reported to have good cyclability, and substituents can tune the redox potential (Fig. 1).[17,18] The classical synthesis of 3,6-diaryl tetrazines requires multi-step synthesis, but recently a cheap and straightforward 1 pot synthesis from corresponding benzonitriles has been reported.[19,20] This new synthesis can dramatically reduce the cost and make DPT attractive as electrode material even though the theoretical capacity is relatively small. We focused on the perfectly planar molecular structure that provides a π-stacked crystal structure that is potentially suitable for reversible insertion/deinsertion of sodium ions into the crystal (Fig. 1b).[21,22] The reversible insertion/deinsertion of metal ions to the crystalline framework is essential in increasing stability and maintaining the constant voltage during charging-discharging. However, the behaviors of such organic materials as the active materials of sodium battery systems are less well known except for a few preceding examples.[4,8,23] Here we will demonstrate in our knowledge for the first time that DPT can be used as reversible cathode material for sodium ion batteries with relatively low overpotential. Additionally, the effect of the crystallinity on the battery performance and the reaction mechanism will be clarified by using ex-situ XRD, FT-IR, and XPS measurements.

2. Experimental

2.1 Methods

DPT (Tokyo Chemical Industry Co., Ltd., 98 %) was purchased and used without further purification. For electrochemical measurements, 70 wt% DPT powder was first mixed in a mortar with 25 wt% acetylene black carbon additive (AB, DENKA Co., Ltd.). The DPT/AB composite powder was kneaded with polytetrafluoroethylene binder (PTFE, Polyflon F-104: Daikin Industries Ltd.) in a weight ratio of 95 : 5. The resulting mixture was formed into disc pellets with a diameter of 10 mm and a total mass of about 30 mg (including about 21 mg of DPT as the active material) and sandwiched between titanium meshes (Thank-Metal Co., Ltd.) to prepare electrode. The electrodes were then dried overnight under a vacuum at 60 °C before assembling the cell. The electrochemical performance of the DPT was evaluated in a 2032 coin-type cell equipped with a polypropylene separator (model 3501; Celgard LLC) against electrolyte (1 M(mol/L) or 1.5 M $NaPF_6$ ethylene carbonate (EC)/dimethyl carbonate (DMC) (1/1 = v/v); Toyama Pure Chemical Industries, Ltd.). All cell assembly was performed in an Ar-filled glove box (dew point < −90 °C). The discharge-charge measurements were performed by a cycle tester (NAGANO & Co., Ltd.) at 25 °C, and the discharge-charge measurements were performed at a constant current density of 0.2 mA/cm^2 (7.48 mA/g).

2.2 Analysis of the electrochemical mechanism

The coin-type cell charged and discharged to the measurement point was quickly transferred into a glove box filled with Ar. The coin-type cell was dismantled, and the pellets were removed and dried in a vacuum dryer for one day. It was then transferred to an airtight cell case for characterization. The pellets in the initial state were the same pellets used in the coin-type cell and were permeated with electrolytes. Powder X-ray diffraction (XRD) was performed using TTRIII (50 kV, 300 mA, Cu-Kα; Rigaku Corporation). FT-IR measurements were performed using FT/IR-4000 (DR-81; JASCO Corporation). Samples were prepared using a part of the pellet and KBr, and a vacuum diffuse reflection measurement system. X-ray photoelectron spectroscopy (XPS) (JPS-9010MC/IV; JEOL Ltd.) was carried out using an Mg-Kα X-ray source. A gold foil was attached to the surface of the pellets, and all energy peaks measured by XPS were calibrated according to the position of the Au $4f_{5/2}$ (87.5 eV) peak.

3. Results and Discussions

3.1 Electrochemical properties of DPT

The electrochemical properties of DPT as a cathode for sodium ion battery were investigated using 1 M $NaPF_6$ EC/DMC (1/1 = v/v) electrolyte (Fig. 2). The initial reversible capacity was 102 mAh/g, which is 90 % of the theoretical capacity assuming one electron reaction (114 mAh/g). A plateau was observed at 1.9–2.1 V vs. Na/Na^+ region during the charge and discharge. This suggests that the discharge-charge reaction is a two-phase equilibrium reaction. As for the cycling characteristics, a sharp decrease was observed in the second reversible capacity, but a gradual decrease was observed thereafter (Fig. 2c). Compared to the reported electrochemical properties of DPT as the cathode of lithium ion batteries, the redox potential was identical, considering the difference between the standard electrode potentials of the anode (Li or Na). There was also only a little difference in overpotential. The significant initial side reaction (higher capacity than the theoretical one electron reaction) observed in lithium ion batteries, reported as the formation of an SEI (solid electrolyte interface), was few observed in sodium ion batteries. The low cycle performance in 1 M $NaPF_6$ EC/DMC (1/1 = v/v) electrolyte could be attributed to the leaching of the active material before and during the discharge-charge process. Actually, dissolution was observed during the cell fabrication, and after the discharge-charge tests, the electrolyte was colored (Fig. S1). The UV-vis spectra of the electrolyte after the discharge-charge cycle did not show the absorption of DPT and were similar to DPT anion created through bulk electrolysis of DPT solution (Figs. S2–S5). In order to solve the leaching problem and

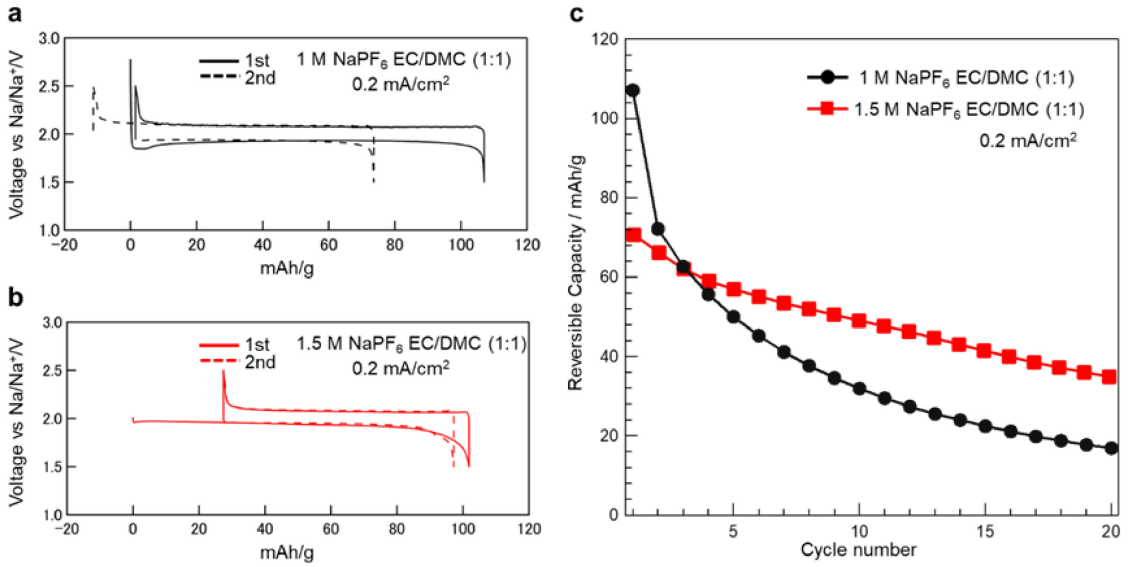

Figure 2. Discharge-charge results at a current density of 0.2 mA/cm^2. **a** discharge-charge curve with 1 M $NaPF_6$ EC/DMC (1/1 = v/v) electrolyte. **b** discharge-charge curve with 1.5 M $NaPF_6$ EC/DMC (1/1 = v/v) electrolyte. **c** cycle characteristics up to the 20th cycle.

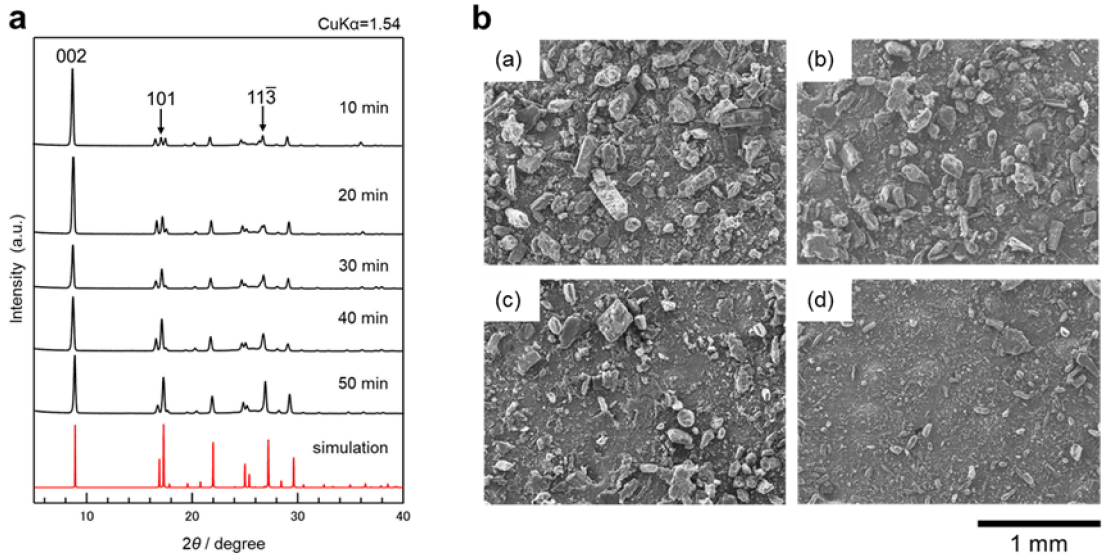

Figure 3. **a** XRD patterns of DPT crystals after AB and DPT mixed in a weight ratio of 70 : 25 were carried out at different ball milling times. The slight difference in the simulated pattern[21,22] and the observed pattern is due to the temperature difference. The Crystal information file used for simulation was measured at 93 K, and the ball-milled samples were measured at 298 K. This will result in a few % lattice expansion. All experiments were carried out at 100 rpm setting; the peak at 002 (8.88°) gradually decreases with ball milling from 10 to 50 min, while the peaks at 101 (17.28°) and 113- (27.18°) gradually increase. **b** SEM images of DPT mixed with AB after ball milling. Ball-milling was conducted under 100 rpm setting. (a) SEM image after 10 min of ball milling. (b) SEM image after 20 min of ball milling. (c) SEM image after 30 min of ball milling. (d) SEM image after 50 min of ball milling. The particle size of DPT gradually decreases.

improve the cycling characteristics, discharge-charge tests employing an electrolyte with a higher concentration of salt (1.5 M $NaPF_6$ EC/DMC (1/1 = v/v)) were conducted (Fig. 2b). The discharge-charge profile was similar as in 1 M $NaPF_6$ EC/DMC (1/1 = v/v) with a plateau at 1.9–2.1 V vs. Na/Na^+. Although an irreversible capacity of about 28 mAh/g was observed during the first charge, the subsequent cycle characteristics have improved compared to 1 M $NaPF_6$ EC/DMC (1/1 = v/v). The reversible capacity was 40 mAh/g, equivalent to 53 % of the initial after the 20th cycle. The higher viscosity of higher concentrated electrolytes may decrease the solubility of both neutral active material and anion radical. Additionally, higher viscosity can kinetically decrease the dissolution rate. The slower dissolution rate due to the kinetic trap was also previously observed by supporting DPT on porous carbon.[17] This method effectively improved the cycle performance of DPT-Li-ion battery and may also be applied to sodium ion battery systems in the future.

Interestingly, the initial crystal size and crystallinity influenced the overpotential accompanying the structure change upon sodium ion insertion into the DPT crystal. The XRD patterns (peak intensity ratio) of DPT change without peak shift when the ball milling time of the DPT-AB mixture is varied (Fig. 3a). The SEM image shows that the DPT crystal is ground, and the crystal size is getting smaller (Fig. 3b). The discharge-charge curve that is assembled from each mixture has shown different overpotentials (Figs. 4 and 5), i.e., a milling time of 20 min showed the smallest overpotential. This can

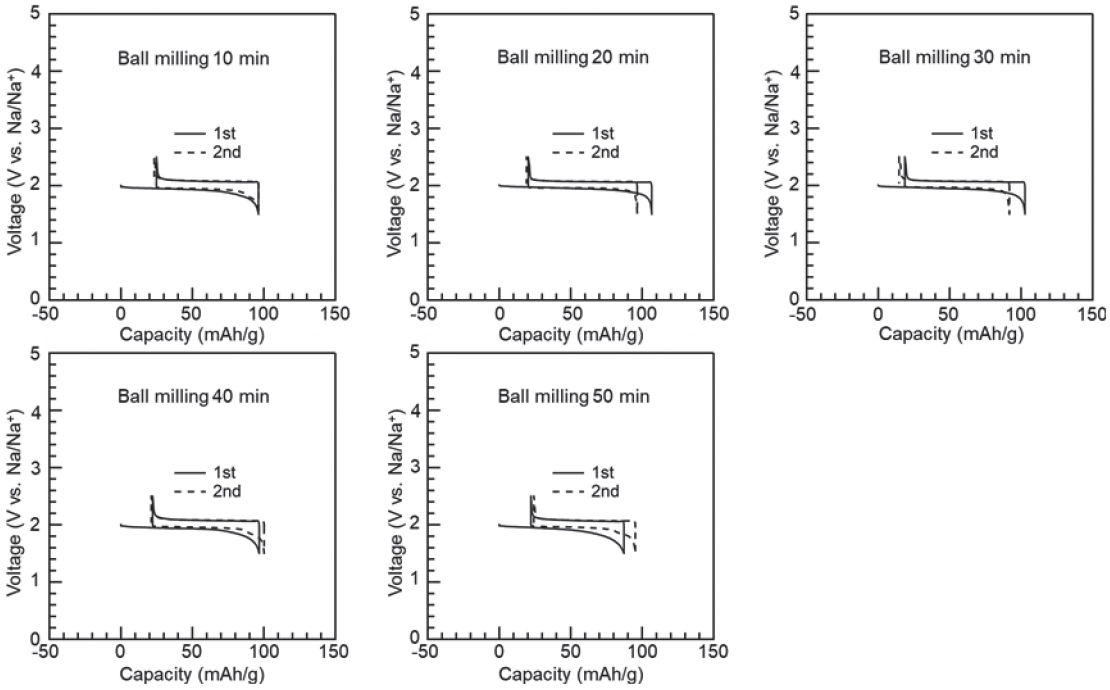

Figure 4. Discharge-recharge curves for the first and second cycles of coin cells fabricated using DPT-AB mixtures with different ball milling times.

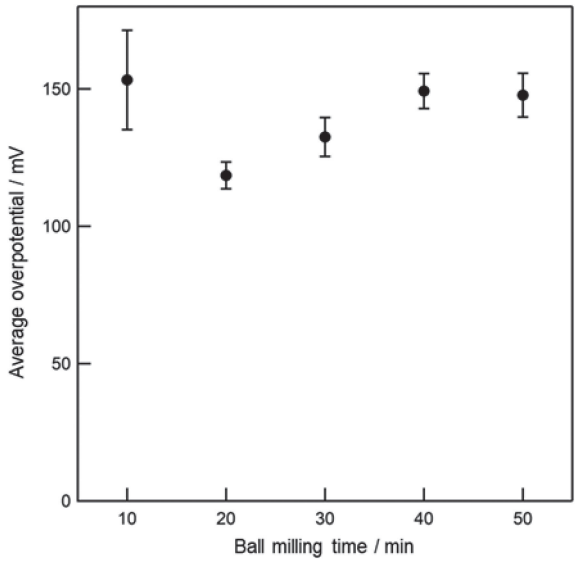

Figure 5. Overpotential during charging and discharging DPT electrodes with different ball milling times. Three coin cells were made for each ball milling time, and charge-discharge tests were carried out. The average overvoltage for each ball milling time was statistically calculated. The average overpotential was the lowest when the ball milling time of 20 min.

be explained by a combination of two factors. 1) Smaller crystal size will result in a shorter diffusion length of sodium ion for insertion, 2) too much grinding will destroy the crystal structure, and the diffusion of sodium ion in the crystal will be inhibited. These two factors also affect the capacity, i.e., the initial discharge capacity increases after grinding 20 or 30 min compared to 10 min and decreases at longer milling time. Obtained results indicate that the crystallinity and crystal size of the material are essential factors for highly efficient reversible reactions using crystalline organic active materials.

3.2 Analysis of electrochemical reaction mechanism

The crystal structure of DPT during the discharge-charge test in a sodium ion battery was investigated by ex-situ X-ray diffraction (XRD) (Figs. 6a and 6b). The intensity of the XRD signal was adjusted based on the peak of PTFE, whose peak intensity is not affected by discharge/charge. The XRD patterns of the initial pellet well agreed with the simulated structure from the previously reported single crystal structure (Fig. S6). The 002 diffraction peak observed at 8.76° decreased upon discharging and perfectly disappeared at the end of the discharge. This 002 peak recovered after charging the cell that is indicating reversibility. Similarly, 17.1°, 17.5°, 21.8°, 24.7°, and 36.1° peaks have also decreased during discharge and recovered after recharge. Conversely, a new peak appeared at 6.88°, 16.1°, 19.9°, 29.5°, and 33.8° during discharge and decreased during recharge. This behavior suggests that sodium ions are reversely incorporated into the crystal lattice of DPT, and a new crystalline phase is created. At this point, the crystal structure of the Na-DPT is not obtained, but this data is consistent with the appearance of a plateau in the discharge-charge curve (Figs. 2a and 2b) and is conclusive evidence of the two-phase equilibrium reaction. The two-phase equilibrium reaction means that the unreacted DPT and the reduced DPT reacted with sodium ions coexist in a phase-separated manner, and the concentration distribution of sodium ions is uneven. Suppose the electrostatic repulsive force between the guest sodium ions in the host structure is strong. In that case, the sodium ion will be distributed evenly in the host, i.e., the DPT anion is well shielding the charge of the sodium ion. The ex-situ XRD spectra of the DPT pellet during the discharge-charge cycle have revealed the structure change upon sodium ion insertion to DPT, and the conversion with a relatively small overpotential suggests that the structural change is occurring smoothly.

Ex-situ FT-IR measurements were performed to elucidate the sites in the DPT molecule that contribute to the redox reaction (Fig. 6c). The FT-IR spectra of the initial pellet showed peaks attributed to DPT (Fig. S7)[24] and other components contained in the pellet. The strong absorption appeared at 850 cm^{-1} and 1780 cm^{-1}

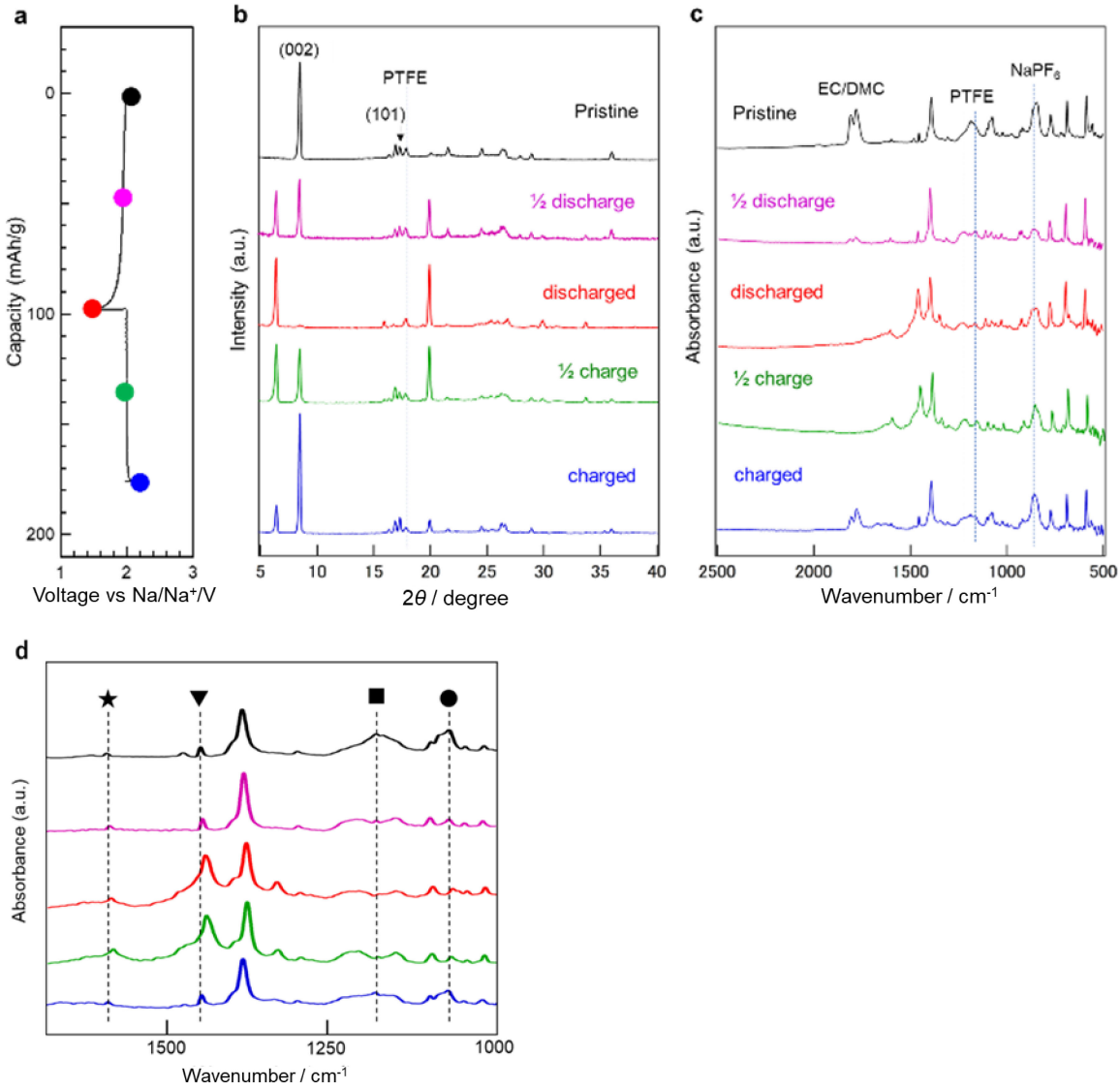

Figure 6. **a** Discharge-charge curves of DPT (1.5 M $NaPF_6$ EC/DMC (1/1 = v/v)), **b** ex-situ XRD patterns of DPT in different charge and discharge states, **c** ex-situ FT-IR spectra of DPT in different charge and discharge states. **d** Enlarged view of the ex-situ FT-IR spectra in **c**. respectively; ●, ■, ▼, ★ indicates 1060 cm^{-1}, 1177 cm^{-1}, 1466 cm^{-1} and 1599 cm^{-1}.

and was found to be electrolyte-derived peaks (Fig. S7).[25] The strength of these peaks depends on the content of the trace amount of electrolyte in each sample and is not a substantial change accompanying the discharge/charge. The peaks at 1155 cm^{-1} and 1212 cm^{-1}, which remain at the end of the discharge, are derived from the PTFE.[26] Several new peaks appeared, and some peaks showed intensity changes during discharging. The new peaks at 1466 cm^{-1} and 1599 cm^{-1} appeared during discharge but decreased after charging, indicating that the reaction was reversible. The peak ratio of 1060 cm^{-1} attributed to C-N-C symmetric stretching and 1177 cm^{-1} attributed to C-H scissor decreased during discharge. Upon charging, the intensity of the peaks returned reversibly to the initial intensity, although not completely. Three strong absorptions at 589 cm^{-1}, 689 cm^{-1}, and 774 cm^{-1} are attributed to the C-H vibrational stretching of the phenyl group. The peak intensity of 589 cm^{-1} is the strongest in the initial state, and during charging, the peak intensity has decreased compared to absorption at 689 cm^{-1}, indicating reversible behavior. These FT-IR results indicate that the substituent phenyl group also is affected by the tetrazine ring redox reaction due to the π-conjugated planer structure. Overall, the FT-IR data guarantees that DPT works as the reversible active material in the sodium ion battery.

To further investigate the electrochemical redox mechanism of DPT, the ex-situ XPS spectra of the electrode during the first discharge-charge cycle were obtained (Fig. 7). In the XPS spectra of the Na 1s spectrums region of the pellet, a peak at 1072.8 eV clearly appeared during discharge and showed the highest peak intensity at the discharge end (Fig. 7a). During recharge, the peak intensity decreased but remained. This suggests the unperfect Na deinsertion or some signal from the dried electrolyte that was observed in the IR spectra. At the same time, in the N 1s region (Fig. 7b), the peak at 401.5 eV in the initial state shifted slightly to the lower energy (399.6 eV) during discharge and then returned to its original position during recharge. This suggests that the nitrogen atom in the tetrazine molecule is negatively charged due to reduction. The C 1s spectrums region was deconvoluted into three prominent peaks (Fig. 7c), the C-(C, H) peak (284.5 eV), the -CF_2- the peak of PTFE (292.5 eV), and the -C-C=N (-C-C=N) peak of the s-tetrazine ring (286.0 eV). The (-C-C=N-) peak strength at 286.0 eV increased significantly upon discharge and reversibly decreased to the initial position after charging.[17] The greater change in the -C-C=N (-C-C=N) peak compared to the C-(C, H) peak suggests that the electron density of the anion is higher at the closer position to the tetrazine ring. The XPS spectra confirmed the reversible tetrazine ring

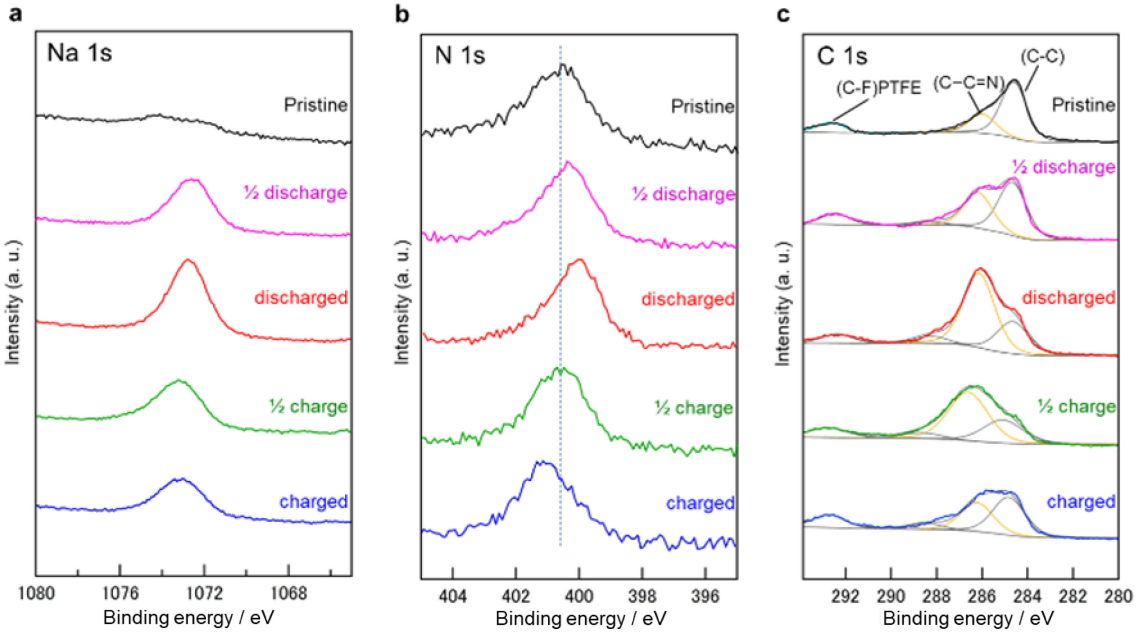

Figure 7. Ex-situ XPS spectra of DPT electrode in different charge states. **a** Na 1s, **b** N1s, and **c** C1s regions.

reduction/oxidation accompanied with sodium ion insertion/deinsertion.

4. Conclusions

DPT showed a reversible discharge-charge behavior as a cathode material for sodium ion battery with a clear plateau around 2 V vs. Na/Na^+. This is the first report of DPT as a sodium ion battery material, and the crystalline structure change upon Na insertion/deinsertion was observed. DPT has a relatively low overpotential for Na insertion, and it could be minimized by optimizing the ball milling time to adjust the crystal size. The XRD patterns show that the 002 crystal plane completely disappears after discharging, and a new crystal phase containing Na is formed. FT-IR and XPS spectra have revealed that C=N and C=C in the tetrazine ring and its vicinity contribute to the electronic reaction. The reversible capacity was 53 % of the initial after the 20th cycle due to severe leaching. This is a task for the future, but potentially by employing porous supports,[17,18] changing the electrolyte, coating,[27] and polymerization[28] should solve this problem. The present results will contribute to the development of novel organic materials for sodium-ion batteries and the analysis of reaction mechanisms of organic electrode materials.

Acknowledgments

This work was finantially supported by the Elements Strategy Initiative for Catalysts and Batteries (ESICB) project (Grant Number JPMXP0112101003), and Leading Initiative for Excellent Young Researchers, Ministry of Education, Culture, Sports, Science and Technology of Japan (MEXT). JSPS KAKENHI Grant No. JP20H00400, JST PRESTO Grant Number JPMJPR18T2, and Kyushu University Platform of Inter-/Transdisciplinary Energy Research (QPIT), and Industrial Science Research Promotion Foundation.

CRediT Authorship Contribution Statement

Jun Watanabe: Data curation (Lead), Formal analysis (Lead), Visualization (Lead), Writing – original draft (Lead)

Masaki Furusawa: Conceptualization (Equal), Data curation (Supporting), Formal analysis (Supporting), Methodology (Supporting), Supervision (Supporting), Writing – review & editing (Supporting)

Kosuke Nakamoto: Conceptualization (Equal), Formal analysis (Equal), Investigation (Supporting), Methodology (Equal), Supervision (Equal), Writing – review & editing (Supporting)

Yuchao Sun: Data curation (Equal), Formal analysis (Supporting)

Masatoshi Tashima: Data curation (Supporting), Formal analysis (Supporting), Visualization (Supporting)

Keiko Yamaoka: Data curation (Supporting)

Seiko Fujiwara: Data curation (Supporting), Formal analysis (Supporting)

Han Seul Kim: Data curation (Supporting), Formal analysis (Supporting)

Shigeto Okada: Conceptualization (Supporting), Funding acquisition (Lead), Methodology (Supporting), Project administration (Equal), Resources (Lead), Supervision (Lead), Validation (Equal), Writing – review & editing (Supporting)

Ken Albrecht: Conceptualization (Lead), Funding acquisition (Equal), Project administration (Lead), Resources (Supporting), Supervision (Lead), Writing – review & editing (Lead)

Data Availability Statement

The data that support the findings of this study are openly available under the terms of the designated Creative Commons License in J-STAGE Data listed in D1 of References.

Conflict of Interest

The authors declare no conflict of interest in the manuscript.

Funding

MEXT: JPMXP0112101003
MEXT: Leading Initiative for Excellent Young Researchers
Japan Society for the Promotion of Science: JP20H00400
Precursory Research for Embryonic Science and Technology: JPMJPR18T2
Kyushu University Platform of Inter-/Transdisciplinary Energy Research (QPIT)
Industrial Science Research Promotion Foundation

References

D1. J. Watanabe, M. Furusawa, K. Nakamoto, Y. Sun, M. Tashima, K. Yamaoka, S. Fujiwara, H. S. Kim, S. Okada, and K. Albrecht, *J-STAGE Data*, https://doi.org/10.50892/data.electrochemistry.21286026, (2022).
1. A. Mauger, C. Julien, A. Paolella, M. Armand, and K. Zaghib, *Materials*, **12**, 1770 (2019).
2. Y. Xu, M. Zhou, and Y. Lei, *Mater. Today*, **21**, 60 (2018).

3. D. Wilkinson, M. Bhosale, M. Amores, G. Naresh, S. A. Cussen, and G. Cooke, *ACS Appl. Energy Mater.*, **4**, 12084 (2021).
4. K. Chihara, N. Chujo, A. Kitajou, and S. Okada, *Electrochim. Acta*, **110**, 240 (2013).
5. W. Xiong, W. Huang, M. Zhang, P. Hu, H. Cui, and Q. Zhang, *Chem. Mater.*, **31**, 8069 (2019).
6. C. Guo, K. Zhang, Q. Zhao, L. Pei, and J. Chen, *Chem. Commun.*, **51**, 10244 (2015).
7. Y. Park, D. Shin, S. H. Woo, N. S. Choi, K. H. Shin, S. M. Oh, K. T. Lee, and S. Y. Hong, *Adv. Mater.*, **24**, 3562 (2012).
8. L. Zhao, J. Zhao, Y. Hu, H. Li, Z. Zhou, M. Armand, and L. Chen, *Adv. Energy Mater.*, **2**, 962 (2012).
9. S. Renault, V. A. Mihali, K. Edström, and D. Brandell, *Electrochem. Commun.*, **45**, 52 (2014).
10. B. Häupler, A. Wild, and U. S. Schubert, *Adv. Energy Mater.*, **5**, 1402034 (2015).
11. C. Luo, G. Xu, X. Ji, S. Hou, L. Chen, F. Wang, J. Jiang, Z. Chen, Y. Ren, K. Amine, and C. Wang, *Angew. Chem., Int. Ed.*, **57**, 2879 (2018).
12. Y. Shan, Y. He, Y. Gu, Y. Sun, N. Yang, H. Jiang, F. Wang, C. Li, D. Jiang, H. Liu, X. Zhu, and S. Dai, *Chem. Eng. J.*, **430**, 133055 (2022).
13. T. Sun, Z.-J. Li, X. Yang, S. Wang, Y.-H. Zhu, and X.-B. Zhang, *CCS Chem.*, **1**, 365 (2019).
14. H. Zhao, J. Wang, Y. Zheng, J. Li, X. Han, G. He, and Y. Du, *Angew. Chem., Int. Ed.*, **56**, 15334 (2017).
15. K. Oka, R. Kato, K. Oyaizu, and H. Nishide, *Adv. Funct. Mater.*, **28**, 1805858 (2018).
16. G. Clavier and P. Audebert, *Chem. Rev.*, **110**, 3299 (2010).
17. D. Min, F. Miomandre, P. Audebert, J. Kwon, and S. Park, *ChemSusChem*, **12**, 503 (2019).
18. D. J. Min, K. Lee, H. Park, J. E. Kwon, and S. Y. Park, *Molecules*, **26**, 894 (2021).
19. C. Li, H. Ge, B. Yin, M. She, P. Liu, X. Li, and J. Li, *RSC Adv.*, **5**, 12277 (2015).
20. J. Yang, M. R. Karver, W. Li, S. Sahu, and N. K. Devaraj, *Angew. Chem., Int. Ed.*, **51**, 5222 (2012).
21. R. Ranjbar-Karimi, CCDC 1580478: *Experimental Crystal Structure Determination*, 2017, DOI: 10.5517/ccdc.csd.cc1q1m5k.
22. K. Momma and F. Izumi, *J. Appl. Crystallogr.*, **44**, 1272 (2011).
23. M. Yao, K. Kuratani, T. Kojima, N. Takeichi, H. Senoh, and T. Kiyobayashi, *Sci. Rep.*, **4**, 3650 (2014).
24. M. Moral, G. García, A. Peñas, A. Garzón, J. M. Granadino-Roldán, M. Melguizo, and M. Fernández-Gómez, *Chem. Phys.*, **408**, 17 (2012).
25. A. V. Cresce, S. M. Russell, O. Borodin, J. A. Allen, M. A. Schroeder, M. Dai, J. Peng, M. P. Gobet, S. G. Greenbaum, R. E. Rogers, and K. Xu, *Phys. Chem. Chem. Phys.*, **19**, 574 (2017).
26. H. Wang, Y. Wen, H. Peng, C. Zheng, Y. Li, S. Wang, S. Sun, X. Xie, and X. Zhou, *Polymers (Basel)*, **10**, 503 (2018).
27. H. Li and H. Zhou, *Chem. Commun.*, **48**, 1201 (2012).
28. Q. Zhao, A. K. Whittaker, and X. S. Zhao, *Materials*, **11**, 2567 (2018).